Colloids and Surfaces B: Biointerfaces 186 (2020) 110603

Contents lists available at ScienceDirect

Colloids and Surfaces B: Biointerfaces

journal homepage: www.elsevier.com/locate/colsurfb

Improved chemotherapeutic efficacy against resistant human breast cancer cells with co-delivery of Docetaxel and Thymoquinone by Chitosan grafted lipid nanocapsules: Formulation optimization, *in vitro* and *in vivo* studies

Sobiya Zafar[a], Sohail Akhter[a,b,c,d,*], Iqbal Ahmad[a], Zubair Hafeez[e], M. Moshahid Alam Rizvi[e], Gaurav Kumar Jain[a], Farhan Jalees Ahmad[a,*]

[a] Nanomedicine Research Lab, School of Pharmaceutical Education & Research, Jamia Hamdard, New Delhi, India
[b] Nucleic Acids Transfer by Non-viral Methods, Centre de Biophysique Moléculaire, CNRS UPR4301, Rue Charles Sadron, 45071 Orléans Cedex 2, France
[c] LE STUDIUM® Loire Valley Institute for Advanced Studies, Centre-Val de Loire Region, France
[d] Yousef Abdullatif Jameel Chair of Prophetic Medical Applications (YAJCPMA), Faculty of Medicine, King Abdulaziz University, Jeddah, Saudi Arabia
[e] Department of Biosciences, Jamia Millia Islamia, New Delhi, India

ARTICLE INFO

Keywords:
Combination chemotherapy
Thymoquinone
Lipid nanocapsules
Endosome escape
Triple negative breast cancer

ABSTRACT

In recent years, multi-targeted chemotherapeutic combinations have received considerable attention in solid tumor chemotherapy. Here, we optimized low-molecular-weight chitosan (CS)-grafted lipid nanocapsules (LNCs, referred to as CLNCs) for the co-delivery of docetaxel (DTX) and thymoquinone (THQ) to treat drug-resistant breast cancer. We first screened size reduction techniques (homogenization vs ultrasonication), and then the 3^3-Box-Behnken design was employed to determine optimal conditions of the final LNCs with the desired quality attributes. Uncoated LNCs had a particle size of 141.7 ± 2.8 nm (Polydispersity index, PdI: 0.17 ± 0.02) with entrapment efficiency (%EE) of 66.1 ± 3.5 % and 85.3 ± 3.1 % for DTX and THQ, respectively. The CS functionalization of LNCs improved the uptake and endosomal escape effect, and led to a significantly higher cytotoxicity against MCF-7 and triple-negative (MDA-MB-231) breast cancer cells. Furthermore, an enhanced antiangiogenic effect was observed with DTX- and THQ-carrying CLNCs in the Chick embryo chorioallantoic membrane (CAM) assay.

1. Introduction

Taxanes, including paclitaxel (PTX, Taxol®) and docetaxel (DTX, Taxotere®), have emerged as promising chemotherapeutics, in mono- and/or combination chemotherapy, for various cancers, including metastatic breast cancer [1]. DTX stabilizes microtubules upon binding with the β subunit of the tubulin protein, and consequently inhibits cell proliferation [1,2]. Commercially available DTX formulations contain high concentrations of Tween 80 and ethanol, which interfere with the protein binding of DTX, resulting in several side effects, including hypersensitivity, hepatotoxicity, nephrotoxicity, and inflammatory, and neuropathic responses [2]. The bulky polycyclic structure of DTX limits its water solubility, and hence its clinical potency [3]. In taxanes, multidrug resistance (MDR) caused by alterations in the apoptotic regulatory proteins, overexpression of Protein kinase B (PKB, or Akt) and phosphoinositide-3-kinase (PI3K) cell proliferators, alteration in tubulins and microtubulin- associated proteins and overexpression of P-glycoprotein (P-gp), is a key issue that needs to be addressed [2,4].

The serious toxicities and challenges associated with conventional chemotherapy has encouraged the exploration of safer and effective alternative strategies. Several reports have demonstrated the beneficial roles of phytomolecules, when combined with conventional chemotherapeutics. These include, a reduction in the side effects [5,6], overcoming the MDR [7,8], reduction in chemotherapeutic dose [9], and therefore, an overall improvement of chemotherapeutic outcome. Thymoquinone (THQ), the bioactive principle isolated from *Nigella sativa* oil, possess anticancer, antioxidant and anti-inflammatory properties [10]. THQ can reduce the toxicity caused by chemotherapeutics, for instance, to ameliorate the ototoxicity and hepatotoxicity induced by cisplatin [6,11], a cardioprotective effect against doxorubicin [12], and prevention of cyclophosphamide induced pulmonary injury [13]. Considering the potential benefits of THQ, it was selected to be combined with DTX, to achieve greater therapeutic efficacy with minimum side effects.

* Corresponding authors at: Nanomedicine Research Lab, School of Pharmaceutical Education & Research, Jamia Hamdard, New Delhi, India.
E-mail addresses: sohailakhtermph@gmail.com (S. Akhter), fjahmad@jamiahamdard.ac.in (F.J. Ahmad).

https://doi.org/10.1016/j.colsurfb.2019.110603
Received 29 May 2019; Received in revised form 16 October 2019; Accepted 18 October 2019
Available online 23 October 2019

Recent studies have introduced the delivery of combined chemotherapeutics using nanomedicines [5,8,14]. A targeted nanomedicine can preferentially localize the payload to the target tissue, controlling the particle size under 200 nm, and modifying the surface with the targeting ligands, thereby achieving enhanced therapeutic effects [14,15]. Previously, we explored the potential of combined PTX and curcumin-loaded pegylated Lipid Nanocapsules (LNCs) to achieve maximum therapeutic efficacy in the Ehrlich Ascites tumor model [8].

In the present report, we developed chitosan (CS) grafted, DTX and THQ co-encapsulating LNCs using oleic acid and phospholipid, stabilized with Poloxamer 188 (P188), an amphiphilic copolymer made up of hydrophilic polyethylene glycol (PEG) and hydrophobic polypropylene glycol (PPG) chains. CS is a biocompatible and biodegradable natural polysaccharide derived from chitin, increasingly being used in drug and gene delivery [16,17]. The chemical structure of CS partially resembles that of hyaluronic acid (HA), but is positively charged, providing a favorable interaction with mammalian cells. CS is capable of targeting the cluster of differentiation 44 (CD44) receptors, commonly overexpressed on cancer cells [14]. In addition to these, CS can degrade or expand in the acidic tumor microenvironment (pH ~6), and in late endosomes and lysosomes (pH ~4-5) [18]. We hypothesized that the CS-nanocapsules (< 200 nm) carrying co-chemotherapeutics can reach the tumor region via enhanced permeability and retention (EPR) effect, and the active targeting of the CD44 receptor on the cancer cells. The encapsulated drug is delivered intracellularly by endosome escape through the proton sponge and fusion effect of CS, and eventually produces efficient cytotoxic effect in the breast cancer cells with reduced toxicity to the normal cells.

2. Material and methods

2.1. Chemicals and reagents

DTX was a gift from Fresenius Kabi Oncology Ltd. (Gurgaon, India). THQ was purchased from Sigma-Aldrich (USA). Lipoid S-PC3 was provided by Lipoid GmbH (Ludwigshafen, Germany). Oleic acid and P188 were obtained from Loba Chemie (Mumbai, India). Low-molecular-weight (LMW) (MW- 110 kDa; DDA- 96 %) CS was provided by Primex ehf (Siglufjordur, Iceland), whereas medium-molecular-weight (MMW) (MW- 190–310 kDa; DDA- 75–85%) and high-molecular-weight (HMW) (MW- 310–375 kDa; DDA- > 75 %) CS were purchased from Sigma-Aldrich (USA). The MTT reagent, 3-(4,5-dimethylthiazol-2-yl)-2,5-diphenyl tetrazolium bromide, was procured from Sigma (USA). All other chemicals and solvents were of analytical grade and were purchased from Qualigens Fine Chemicals (Mumbai, India).

2.2. Formulation development

LNCs were prepared by employing two different size reduction techniques—high-speed homogenization and ultrasonication. The steps followed were common between the two techniques, except at the final stage when external high energy was applied. DTX and THQ (1:2 w/w) were dissolved in a mixture of oleic acid:phospholipid (Lipoid S-PC3; maintained at 55–60 °C), and solubilized in ethanol. This served as the organic phase, and was subsequently injected into the aqueous phase containing P188. The contents were continuously stirred using a magnetic stirrer at 2500 rpm, resulting in ethanol evaporation, leaving behind the drug-loaded uncoated LNCs (ULNCs). The ULNCs were passed through SilentCrusher (Heidolph Instruments S, Germany) operating at a speed of 15000–45000 rpm, for 2–5 cycles. Acoustically assisted LNCs were fabricated using a 30 kHz UP50H® ultrasonic processor (Hielscher-Ultrasound Technology, Germany) at 40–60% amplitude for 1–5 min. The effects of concentration of the emulsifying agent (P188), liquid lipid-to-solid lipid ratio (LL:SL ratio), and sonication time (ST) on particle size and entrapment efficiency (%EE) were further investigated using the quality by design methodology.

Equal volumes of ULNCs were incubated in 0.1 %(w/v) of three different molecular weight (MW) CS, and were maintained with mild stirring for 5–6 hrs. The chitosan-coated LNCs (CLNCs) were centrifuged (Beckman Coulter LE80, United States) at 50,000 *g* for 30 min, the nanocapsules were separated, washed properly with distilled water, and dispersed in the solution of cryoprotectant (sucrose, 5 %w/v) for freeze drying using the lyophilizer (Triad TM, Labconco, MO).The final product was stored in tight containers at 4 °C for further use.

2.3. Formulation design and optimization

A 3-factor, 3- level Box–Behnken statistical design (BBD) was employed using the Design-Expert software (DES) (Design-Expert 11.1.0, State-Ease Inc., Minneapolis, USA) [19], to obtain the most suitable formulation, with the desired particle size, and %EE. BBD suggested 17 runs consisting of 12 factorial points, and 5 replicates of the central point by defining the independent variables at three levels: low (−1), basal (0) and high (+1), as shown in Table S1. The independent variable LL:SL ratio varied from 2:3 to 3:2, the P188 concentration from 2 % to 4 % w/v, and ST from 2 to 6 min. The responses observed included particle size (nm) (R1), %EE for DTX (R2) and %EE for THQ (R3). Analysis of variance (ANOVA) established the statistical validation of the polynomial equations obtained by DES. The resultant experimental values of the responses were compared with the predicted values for the optimized formulation.

2.4. Characterization of LNCs

2.4.1. Particle size and zeta potential

The particle size, polydispersity index (PdI) and zeta potential of the LNCs were measured using the Zetasizer (Nano ZS, Malvern Instruments, Malvern, UK). For the detailed method, please refer to the Supplementary file, section 1.1.

2.4.2. Determination of encapsulation parameters

In order to determine %EE and drug loading (DL %), samples (10 mg) were accurately weighed and dissolved in methanol to extract the drug from the lipid matrix. The mixture was centrifuged at 50,000 *g* for 15 min. The supernatant was appropriately diluted with acetonitrile (ACN):water (50:50), and the amount of DTX and THQ in the supernatant was determined with the High-Performance Liquid Chromatography (HPLC) method, using the equations mentioned below. Chromatographic analysis for the simultaneous estimation of DTX and THQ was performed using the Alliance HPLC system (e2695 Separation module, Waters, New Delhi, India), equipped with variable wavelength programmable photodiode array detector (PDA) (for details of method, please refer Supplementary file, section 1.2). In this method, water:ACN (45:55) was used as the mobile phase. Representative chromatogram is provided in figure S1. The calibration curve was found to be linear over a concentration range of 0.3125–10 μg mL^{-1}, and 0.625–20 μg mL^{-1}, with a regression coefficient (r^2) value of 0.991 and 0.994, and retention times of 3.5 ± 0.03 min and 5.2 ± 0.05 min, for DTX and THQ, respectively.

$$EE(\%) = \frac{\omega_i - \omega_F}{\omega_i} \times 100$$

$$DL(\%) = \frac{\omega_i - \omega_F}{\omega_t} \times 100$$

Where ω_i, ω_f, ω_t stands for the total amount of drug added during the preparation of the LNCs, amount of drug measured in the supernatant, and the total weight of LNCs used for analysis, respectively.

2.4.3. Endosome escape study

The endosome escape study was performed to select the type of CS, LMW, MMW, or HMW, which could mediate efficient cytosolic delivery

of the therapeutic agent, using the reported method with slight modifications [20]. Briefly, blood samples collected from Wistar rat were centrifuged at 500 × g for 10 min, the plasma was gently aspirated, and the cells were washed with 150 mM NaCl solution. The supernatant obtained upon centrifugation (500 × g for 5 min) was replaced with phosphate-buffered saline (PBS) pH 7.4, evenly (1 mL each) split into two microcentrifuge tubes (MCT), corresponding to each pH to be tested, and again centrifuged. The marked lines were filled with the buffer of the appropriate pH. Erythrocytes were then diluted 50 times with the buffer of the corresponding pH. Each stock solution was pipetted (50 µL) into MCT in triplicate, and 950 µL of diluted erythrocytes was added. For the positive and negative controls, 20 % Triton X-100 and phosphate buffer at the same pH to be tested, were used. The MCTs were incubated at 37 °C for 0.5, 1, 1.5 and 2 h, and centrifuged for 5 min at 500 × g to pellet intact erythrocytes. The absorbance of the supernatant was recorded at 510 nm.

2.4.4. Physicochemical characterization of LNCs

Transmission and Scanning electron microscopy (TEM & SEM) were performed to determine the morphological characteristics of the ULNCs and CLNCs. Fourier Transform Infrared Spectroscopy (FT-IR) was performed using a FT-IR spectrometer (FTS-135, BIO-RAD, USA), X-Ray Diffraction (XRD) analysis using a X-ray Diffractometer (Model: PaNalytical X-ray powder diffractometer) and thermal analysis by differential scanning calorimetry (DSC) (PerkinElmer, USA; Pyris software v 6.0) was carried out to analyze the physical state of the drugs and, its distribution in the LNCs matrix, interactions between the drugs, excipients and the LNCs. For details please refer to supplementary document, section 1.3, 1.4, 1.5 and 1.6.

2.5. In vitro release study

DTX and THQ release profiles from LNCs was determined under sink conditions, and release kinetics were evaluated using different kinetic models: zero order, first order, Higuchi and Korsmeyer-Peppas model, and the r^2 was calculated. Detailed methodology is elaborated in the Supplementary file, section 1.7.

2.6. Hemolytic toxicity assay

To perform the hemolysis assay, blood was collected from a healthy rat into K2-EDTA-coated Vacutainer tubes, and centrifuged at 500 × g for 20 min. After discarding the plasma, the erythrocytes were washed with normal saline (NS) to remove the serum proteins. NS was added to the erythrocytes to obtain erythrocyte stock dispersion (ESD) of 50 % hematocrit. ESD (0.1 mL) was added to 3 mL of NS (negative control), double distilled water (DW) (positive control), and CLNCs at predetermined concentrations. The samples were shaken gently, incubated (Incubator Shaker, SI6R, Shel Lab, USA) at 37 °C for 1 h, and then centrifuged at 1000 × g for 15 min. The absorbance of the supernatant was calculated at 540 nm using the Ultraviolet-Visible (UV–VIS) spectrophotometer. The experiment was performed in triplicate, and the percentage hemolysis was estimated using the following equation:

$$Hemolysis(\%) = \frac{Abs_{sample} x100}{Abs_{control}}$$

Where, Abs_{sample} is absorbance of sample, and $Abs_{control}$ is the absorbance of the positive control.

2.7. In vitro cell viability assay

To study the cytotoxic effect of DTX, THQ, single drug-loaded LNCs (DTX-LNCs), ULNCs, and CLNCs, the 3-(4, 5-dimethylthiazol-2-yl)-2, 5-diphenyltetrazolium bromide (MTT) assay was performed using the MCF-7 and MDA-MB-231 cell lines [2]. First, 5000 cells/well were seeded in 96-well flat-bottomed plates (Falcon Plate, Corning Costar, USA), and incubated for 24 h to allow cell attachment. After 24 h, the growth media was removed from each well, and 180 µL of media containing the test solutions were added. Untreated cells were used as controls. After incubation for 24 and 48 h, 20 µL of 5 mg/mL MTT in PBS was added to each well, and incubated for 4 h. Next, the medium was removed, and 150 µl of dimethyl sulfoxide (DMSO) was added to each well and the plate was shaken for 5 min. The absorbance was measured at 570 nm using a microplate reader (LMR-340 M, Labexim International, Austria). Percentage cell viability was calculated as follows:

$$Cell\ Viability(\%) = \frac{Abs_{sample} x100}{Abs_{control}}$$

Where, Abs_{sample} stands for the absorbance of sample, whereas $Abs_{control}$ is the absorbance of the control.

2.8. In vivo anti-angiogenesis assay

The *in vivo* antiangiogenic activity was evaluated using the chick embryo chorioallantoic membrane (CAM) assay, using a previously reported method with slight modifications [21]. The benefits of the CAM model over animal models include low cost, ease of culture, and easy observation of neovascularization (the embryo being still alive) without sacrificing the animals [22]. Fertilized chicken eggs (10 per group) were incubated at 37 °C, at a relative humidity (RH) of 60–70%, and a square window opened on day 3. Next, 2–3 mL of albumen was removed to allow CAM detachment from the shell, and the eggs were returned to the incubator after sealing the window with a laboratory film. Stock solutions of DTX and THQ prepared in 100 % DMSO were further diluted to 1 mL with 0.9 % NaCl, producing working solutions of 3.3 µM and 6.6 µM for DTX and THQ in 0.1 % DMSO/ NaCl, respectively. Ten microliters of the test samples were applied to the CAM of the developing embryo on day 9. CAMs were examined daily until day 11, and photographed. The time dependence of the response of the CAM blood vessels to different treatment groups, was evaluated at 24 and 48 h post incubation, and the percentage inhibition was calculated.

3. Results and discussion

3.1. Formulation development

The nanoemulsion technique was employed for loading DTX and THQ into the formulation using Poloxamer as surfactant, which imparted physical stability to the LNCs, enhanced the %EE of the lipophilic drugs, and suitable for administration via the parenteral route. CS, a biodegradable and biocompatible polymer, can provide additional benefits such as, enhanced circulation of the nanocapsules, and also mediate the endosome escape phenomenon, concentrating a greater proportion of nanoparticles within the cell [16].

To exploit the full advantages of EPR in cancer nanomedicine, the particle has to be controlled within the size range of 20–200 nm [15]. For this purpose, two different techniques investigated were, the high-speed homogenization (HSH), and ultrasonication. LNCs were subjected to 5 cycles of HSH with varying speeds, and the effect on particle size and PdI was determined (Fig. 1.A). The two major forces responsible for particle size reduction in rotor-stator systems are the mechanical impingement against the wall due to high fluid acceleration, and the shear stress generated in the gap between rotor and stator, due to the rapid rotation of the rotor. The particle size can be altered by controlling the emulsification intensity (power), and by the residence time the emulsion droplets stay in the shearing field [23]. The particle size ranged from 164 to 334 nm, with the PdI of 0.39 to 0.70 for LNCs produced using HSH (figure S2). It was observed that the lower mixing speeds exerted insufficient mixing energy producing greater mean particle

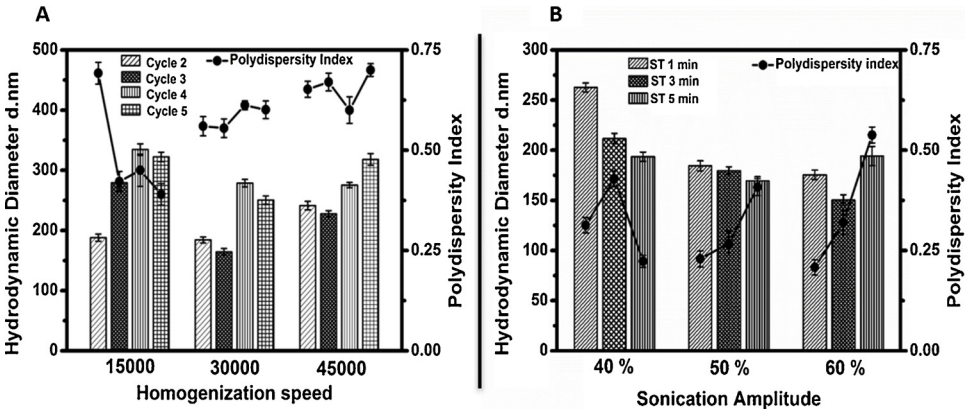

Fig. 1. Effect of (A) Homogenization speed and number of cycles; (B) Ultrasonication time and power amplitude on LNCs hydrodynamic diameter and PdI. Values are reported as mean ± S.D (n = 3).

sizes. At high homogenization speeds of 45,000 rpm, the particle sizes were found to be larger that may be due to overprocessing of the system. The input of excess energy increased the knocking frequency between the particles resulting in coalescence and hence the development of larger particles. Furthermore, it was also observed that the particle size decreased with the increase in number of cycles from 2 to 3, as the higher homogenization speed and the cycle provided higher energy for breaking the particle agglomerates into smaller units [24]. PdI was not significantly altered with higher homogenization speed or number of cycles, however, a significant difference was observed with the speed of 15,000 rpm, and increasing the number of cycles from 2 to 5, but this formulation was unstable. Size reduction using the rotor-stator system is generally less efficient, as the mean power density is relatively low and the mean residence time of the emulsion droplet is longer in the dispersing zone of the rotor-stator devices. This causes the operating forces to act longer than the minimum time required for the droplet break-up [23]

In the ultrasound assisted particle size reduction, the ultrasound waves transferred through the liquid medium produced cavitation where the formation, growth and implosive collapse of the microbubbles/cavities occurred. Due to the transient collapse condition, localized hot spots comprising of high temperature and pressure are created that initiates the desired physical transformation during emulsification. Thus, the two mechanisms for size reduction based on ultrasonication include- i) generation of droplets in the acoustic field; ii) creation of intense turbulence and microjets during asymmetric cavity collapse resulting in the break up, and dispersion of droplets in the continuous phase [25,26]. The effect of power amplitude and the sonication time was studied to obtain uniform small sized particles (Fig. 1.B). It was observed that on increasing the power amplitude from 40 % to 60 %, the particle size decreased from 262.7 ± 4.49 nm to 150.3 ± 5.34 nm (figure S3). This was due to the fact that the high amplitude dissipates more energy to the system, producing a significantly higher cavitation collapse pressure at the end of asymmetric cavity collapse [26]. The increase in sonication time increases the acoustic cavitation and therefore, decreases the particle size. However, with a further increase in sonication time the droplet coalescence is initiated which increases the particle size [27]. Since the particles obtained with the ultrasound assisted cavitation were found to be smaller and more stable than those produced with HSH, it was selected for the further development of LNCs.

3.2. Formulation optimization

Quality by design (QbD) entails achieving certain predictable quality given desired and predetermined specifications. An important component of QbD is to understand the factors and their interaction effects using a desired set of experiments [28]. To understand this, experimental statistical designs were used to develop successful techniques, which were utilized to obtain a robust formulation with optimal characteristics. Experimental designs and statistics are efficient tools to control and optimize the process and formulation variables. The experimental design limits the number of trials and the burden of time and cost, and still provides significant results. Therefore, in the present study, BBD, a response surface methodology (RSM) approach, has been utilized. BBD offers a better approach to evaluate the main effects and the interaction effects of the independent variables on the formulation characteristics [29].

Here, LL:SL ratio, P188 concentration (%) and ST (min) were chosen as independent variables with R1 (particle size), R2 (%EE of DTX) and R3 (%EE of THQ) as dependent variables. The software generated 17 trials and response data for all experiments is compiled in table S2.

Selection of the model source, for the responses, was based on the sequential model sum of squares, lack of fit, and model summary statistics. The design suggested the Quadratic model for the response data. The multiple regression terms were analyzed and gave a "Predicted r^2" value of 0.7919, 0.9493 and 0.8886, which were found to be in reasonable agreement with the "Adjusted r^2" value of 0.9644, 0.9703 and 0.9470 for R1, R2 and R3 respectively. Adequate precision measures the signal to noise ratio. A ratio greater than 4 is desirable. The ratios of 26.9027, 23.7366, and 18.0920 were observed for R1, R2 and R3, respectively, indicating an adequate signal. This suggested that the model could be used to navigate the design space. The polynomial equations which represented the quantitative effects of process variables, and their interaction effects on the responses, were as follows-

$$\text{Particle size} = +126.60 + 10.78\ *A - 10.83\ *B + 19.27\ *C + 24.08\ *A*B + 1.13\ *A*C - 16.53\ *B*C - 5.14*A2 + 29.56*B2 + 44.92*C2 \quad (1)$$

$$\%\ \text{EE (DTX)} = +57.01 + 3.23\ *A - 3.76\ *B - 7.39\ *C - 2.52\ *A*B - 0.7225\ *A*C - 3.54\ *B*C - 3.53*A2 + 0.3068*B + 3.02*C2 \quad (2)$$

$$\%\ \text{EE (THQ)} = +74.89 + 3.13\ *A - 3.98\ *B - 8.07\ *C - 2.58\ *A*B - 1.32\ *A*C - 4.51\ *B*C - 4.59*A2 + 0.1290*B2 + 3.35*C2 \quad (3)$$

where A, B and C are the descriptors for different independent variables, as described in table S1.

The positive sign of the coefficient in the equations generated, indicated a synergistic effect of the factor on the response, while the negative sign represented an antagonistic relationship. From the equations it can be observed that, the factor 1 (LL:SL ratio) had a positive effect while the factor 2 (P188 Concentration) had a negative influence on all the responses studied. The factor 3 (ST) displayed a positive effect on R1, however, a negative effect was observed on the other two responses. With the critical analysis of the 3D response surface plots (figure S4), it was observed that increasing factor 1 caused a

non-linear increase in the particle size and % EE. The increased concentration of the lipid phase increased the particle size due to the higher viscosity of the lipid phase, that reduced the diffusion rates of the solute molecules [30]. However, a suitable balance between the LL and SL concentrations has to be maintained, as increased amount of SL may cause mixtures to exhibit more prefect crystalline lattice that may increase the drug expulsion on storage, and the excessive amounts of LL could enlarge the gaps generated by structural differences between the LL and SL destroying the disordered structure of the system, and hence its stability [30,31]. The particle size significantly decreased on increasing the P188 concentration up to a certain limit, and then increased with the further increase in P188 concentration. This may be due to the reduction in the interfacial tension between the lipid and aqueous phase, while a simultaneous decrease in %EE was observed due to the reduced size which contained less lipid and hence entrapped drug [8]. The increase in ST caused the particle size to decrease, but increased with further increase in ST. The initial decrease in the particle size can be attributed to the increased acoustic cavitation. However, after a certain point, the kinetic energy increased remarkably, destabilized the steric barrier assisted by surfactant, and resulted in particle aggregation causing increased particle size [29]. A significant decrease in %EE was observed with the increase in ST. The apparent decrease in R2 and R3 was due to deformation in the lipidic structure with higher sonication time, resulting in leaching of the loaded drug into the aqueous medium.

We studied the influence of different independent factors on the responses, and their levels were determined using a computer optimization process and a desirability function, RSM. The analysis of the response variable for the optimal formulation with minimum particle size, maximum % EE, and desirability (near to 1) was selected and prepared in triplicate to confirm the validity of the optimization procedure. The results for the optimized values for different factors are summarized in table S3. The optimum conditions to produce LNCs were found to be a 3:2 ratio of LL:SL, 2 % of P188, with ST of 2 min. The optimized ULNCs exhibited a mean particle size of 141.7 ± 2.8 nm with a PdI of 0.17 ± 0.02, and %EE of 66.1 ± 3.5 % for DTX, and 85.3 ± 3.1 % for THQ.

3.3. Characterization of LNCs

3.3.1. Particle size and zeta potential

The mean particle size for the ULNCs, LMW CS coated LNCs (CL-LNCs), MMW CS coated LNCs (CM-LNCs) and HMW CS coated LNCs (CH-LNCs) was found to be 141.7 ± 2.8, 175.3 ± 4.4, 184.5 ± 4.7, 208.7 ± 7.1 nm, respectively, while the PdI was 0.17 ± 0.02, 0.12 ± 0.06, 0.17 ± 0.08, 0.25 ± 0.03, respectively (Fig. 2.A). Zeta potential values were found to be -8.17 ± 0.1 mV (ULNCs), 16.9 ± 0.5 mV, 4.94 ± 0.3 mV, and 26.1 ± 0.5 mV for CL-LNCs, CM-LNCs and CH-LNCs, respectively (Fig. 2.B). The increase in particle size and change in zeta potential from negative to positive charge indicated the coating of different MW CS on the surface of LNCs. Shorter polymer chains with decreased MW develops nanoparticles with a smaller size [32]. CS with higher degree of deacetylation (DDA) results in greater zeta potential due to higher charge density of the more deacetylated chitosan [16].

3.3.2. Determination of encapsulation parameters

In the final optimum formulation, the %EE of DTX and THQ in ULNCs and CLNCs ranged from 66.1 ± 3.5%–67.1 ± 4.0 %, and 85.3 ± 3.1%–88.0 ± 4.4 %, respectively, while the drug loading (%) ranged from 2.8 ± 0.4%–4.3 ± 0.4 %, and 4.4 ± 0.4%–7.7 ± 0.4 %, respectively (Table 1). The experimental data revealed that CS improved the %EE of DTX and THQ in the LNCs. This could be attributed to the fact that the CS could coat the surface of the nanocapsules, which prevented the leakage of DTX and THQ from the nanocapsules.

3.3.3. Endosome escape study

Facilitating endosome escape is an important strategy for the selective and efficient delivery of biologicals in cancer therapy. Nanocarriers are primarily taken into cells via endocytic pathways and subsequently the endocytic vesicular content is trafficked to enter either recycling endosomes to undergo exocytosis, or late endosomes to undergo degradation, limiting the delivery of therapeutic agents to the intracellular target. With mounting evidence on efficient gene delivery with endocytic pathway modulation, recent studies demonstrate the paramount importance of the endosome escape effect for the efficient intracellular delivery of small molecules. Several mechanisms such as pore formation in the endosomal membrane, the pH buffering effect (the proton sponge effect), fusion in the endosomal membrane and photochemical disruption of the endosomal membrane have been proposed for the efficient endosome escape of the nanoparticles [33–35]. Cationic polymers with pH buffering properties have been extensively used for endosomal disruption mediated delivery of biologics into the cytosol. The protonation leads to the extensive inflow of ions and water into the endosomal compartments, resulting in the rupture of the endosomal membrane releasing the entrapped components. CS with its biodegradable, biocompatible and non-immunogenic nature can be used to mediate the endosomal escape effect resulting in the conducive delivery of biologics intracellularly [17,18]. The developed LNCs with the surface coating of CS could be a promising vehicle for the delivery of DTX and THQ within the cells, providing efficient chemotherapy.

The *in vitro* endosome escape study was carried out at two different pH (pH 5.5, pH of endosomes, and pH 7.4). As evident from Fig. 3, the hemolysis (%) was negligible at pH 7.4 for all the LNCs, while greater hemolysis with different MW CS was observed at pH 5.5. The slightly acidified medium increased the zeta potential of the nanocapsules,

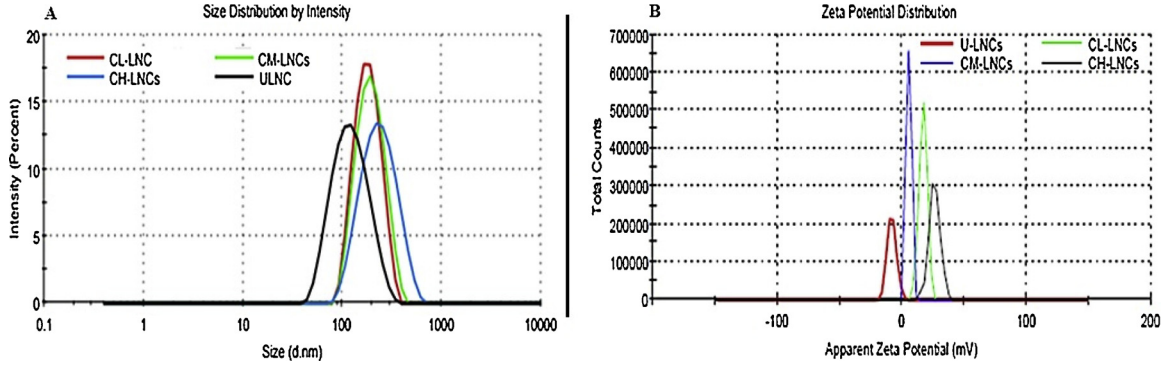

Fig. 2. Effect of different molecular weight chitosan on (A) particle size and (B) Zeta Potential of the LNCs. The increase in particle size and change in zeta potential from negative to positive for CLNCs compared to ULNCs demonstrates efficient coating of CS on the surface of LNCs. Each measurement has been performed three times.

Table 1
Physicochemical characterization of ULNCs and CLNCs (Data is presented as mean ± S.D (n = 3)).

Formulations	Particle size (nm)	Polydispersity index (PdI)	Zeta potential (mV)	% Entrapment efficiency		Drug loading (%)	
				DTX	THQ	DTX	THQ
ULNCs	141.7 ± 2.8	0.17 ± 0.02	−8.2 ± 0.1	66.1 ± 3.5	85.3 ± 3.1	2.8 ± 0.4	4.4 ± 0.4
CL- LNCs	175.3 ± 4.4	0.12 ± 0.06	16.9 ± 0.5	65.6 ± 4.1	86.2 ± 2.1	3.6 ± 0.7	5.2 ± 0.2
CM- LNCs	184.5 ± 4.7	0.17 ± 0.08	4.9 ± 0.3	67.9 ± 3.3	86.2 ± 4.6	3.9 ± 0.3	5.4 ± 0.5
CH- LNCs	208.7 ± 7.1	0.25 ± 0.03	26.1 ± 0.5	67.1 ± 4.0	88.0 ± 4.4	4.3 ± 0.4	7.7 ± 0.4

ULNCs: Uncoated lipid nanocapsules; CL- LNCs, CM- LNCs, and CH- LNCs are Low-, medium-, and high-molecular-weight chitosan coated lipid nanocapsules, respectively.

which increased the binding efficiency to the cell membrane, and hence the greater uptake of nanocapsules [16]. At pH 5.5, the ULNCs exhibited 22 ± 3.2 % hemolysis at 2 h, while the CL-LNCs, CH-LNCs, CM-LNCs exhibited 85.1 ± 2.5 %, 77 ± 3.9 % and 58.1 ± 3.5 % hemolysis, respectively at 2 h. The results indicated that all the three forms of CS grafted LNCs are effective fusogenic or lysogenic NPs, compared to U-LNCs. CL-LNCs, CM-LNCs and CH-LNCs, owing to the higher buffering capacity of CS, and exhibiting a proton sponge effect ultimately leading to swelling and finally lysis of the endosomal vesicles, allowed the release of payload and/or LNCs into cytosol [17]. The LNCs coated with LMW CS (CL-LNCs) was selected for further studies as it exhibited the smallest particle size, and efficient endosome escape effect.

3.3.4. Physicochemical characterization of LNCs

As evident from TEM and SEM images, the ULNCs exhibited particle sizes of 80–150 nm, which corroborated with the results obtained by DLS (Fig. 4.A1, 4.A2). CS coating was well depicted with a well-defined light boundary around the ULNCs (Fig. 4.A2). Spherical shaped nanoparticles with smooth surface morphology were observed (Fig. 4.B1, 4.B2). Particles were slightly agglomerated that could be ascribed to the sticky nature of lipid of the carriers.

The FT-IR analysis was performed to study the interactions between different functional groups of the drugs and the excipients [36]. An intense band was observed for DTX at 1700 cm^{-1}, 3740 cm^{-1}, and 1515 cm^{-1} corresponding to C═O stretching, O−H stretching and N−H plane bending, respectively (figure S5.A). The FT-IR scan of THQ (figure S5.B) showed diagnostic peaks at 1654 cm^{-1} (C═O stretching), multiple bands at 1525-1461 cm^{-1} (C═C of benzene ring), and doublet at 1367-1377 cm^{-1} which signified isopropyl group containing tertiary carbon. For CS, the medium intensity peaks were observed at 1540 cm^{-1} that signified N−H bending mode, 1379 cm^{-1} for C–N vibration of amino group. A strong band at 1024 cm^{-1} signified CO in the ether group (figure S5.D). Some shift or disappearance of the diagnostic peaks in FT-IR of ULNCs (figure S5.E) and CLNCs (figure S5.F) suggested the formation of some non-covalent bonds such as, hydrogen bonds and the hydrophobic interactions, between the drug and excipients that facilitated the effective solubilization and entrapment of the therapeutic agents within LNCs [2].

The XRD data showed drugs (DTX and THQ) in their crystalline state, with characteristic peaks between 8.78° - 21.68° two-theta for DTX, while 8.7° - 45.7° two-theta for THQ. CS and lipid exhibited a single diffraction peak at 20.5° and 21.6° two-theta, respectively. Broad diffraction peaks, with no drug peaks, were observed in the XRD pattern of CLNCs (figure S6) indicating the molecular dispersion of both the drugs in the nanocapsules.

DSC thermograms at 153.6 °C and 50 °C corresponded to the melting point of DTX and THQ, respectively. The broad endothermic peak at 78.7 °C, with the absence of any endothermic peaks of drugs in the thermogram of CLNCs, suggested that the drugs are either completely dissolved or molecularly dispersed within the lipid matrix of the LNCs (figure S7).

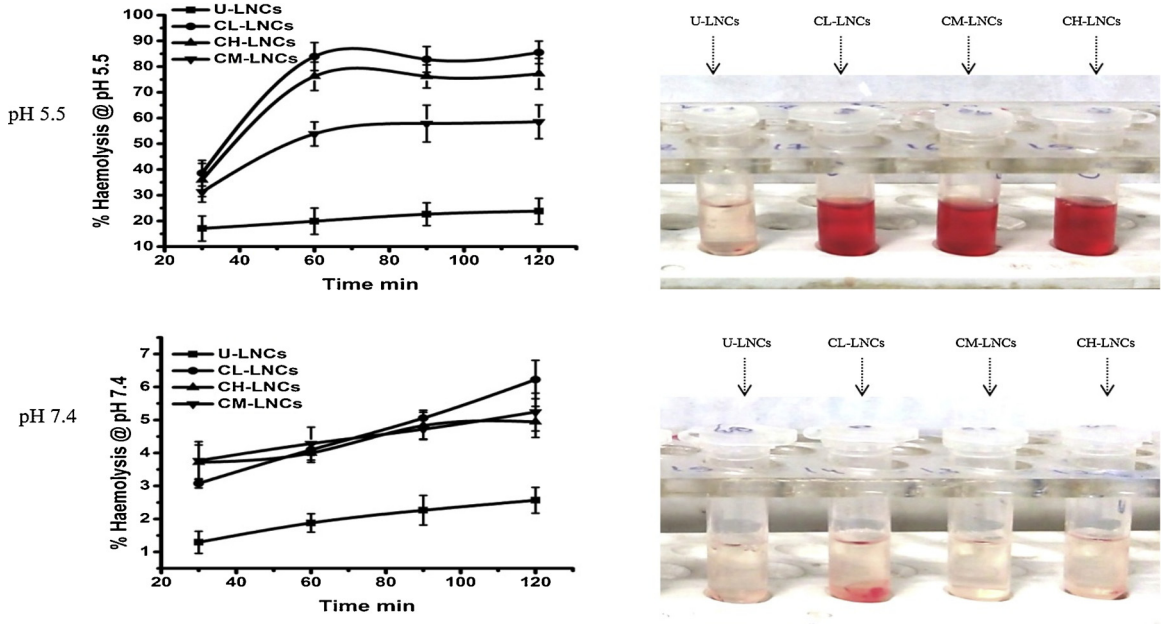

Fig. 3. Endosome escape study at different pH values. The CLNCs exhibited greater hemolysis (intense red color) compared to ULNCs at endosomes pH (pH 5.5) while negligible hemolysis was observed at physiological pH (pH 7.4). Values are reported as mean ± S.D (n = 3) (For interpretation of the references to colour in this figure legend, the reader is referred to the web version of this article.).

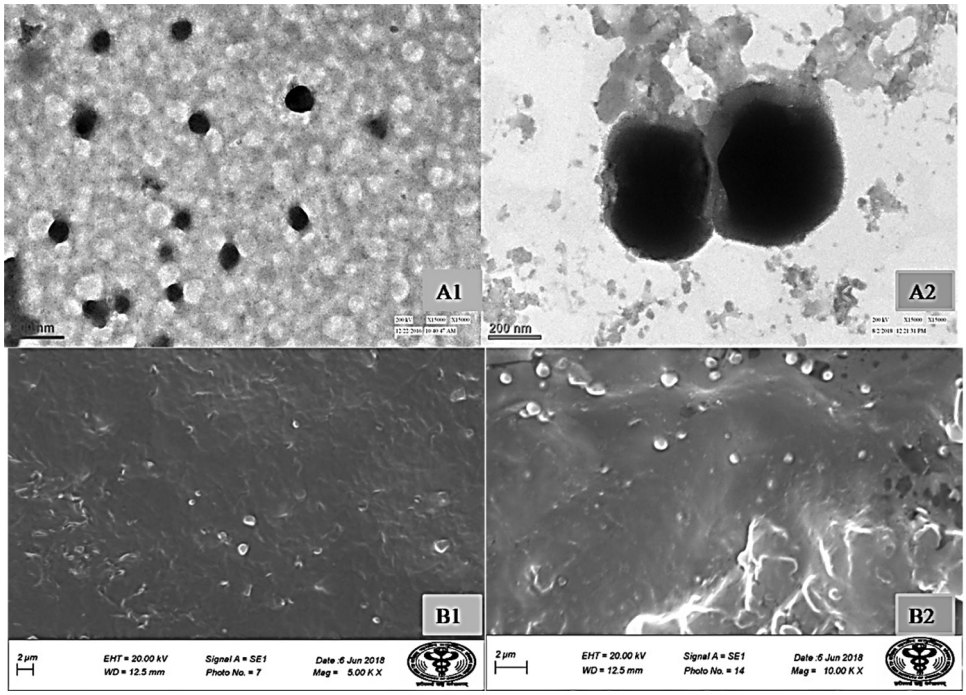

Fig. 4. Transmission electron microphotographs (A1 & A2) and Scanning Electron microscopy images (B1 & B2) of ULNCs and CLNCs.

3.4. In vitro release study

As evident from the release curve (Fig. 5), a burst release of about 23 ± 2.1 % and 37.1 ± 2.4 % was observed for DTX and THQ, respectively, in the initial 2 h, whereas in the next 24 h, they were released in a sustained manner at approximately 42.2 ± 2.1 % and 75.9 ± 2.3 %, respectively. In the first 4 h, little difference was observed in DTX release from DTX ULNCs and DTX CLNCs. Following this, a significant improvement in DTX release was observed from DTX CLNCs. Here, it is noteworthy to mention that, irrespective of the kind of LNCs, the release percentage of THQ is significantly higher than that of DTX for up to 24 h (Fig. 5). The increased release profile from CLNCs is attributed to CS induced hydrophilic surface over the LNCs, and the increased diffusion pores over time. In case of drug molecules, the LNCs allows lower MW and lower lipophilic drugs (THQ; log P: 2.2 & molecular weight: 164.201 g/mol) to be released prior and faster than the higher MW and higher lipophilic drugs (DTX; log P: 4.1 & molecular weight: 807.89 g/mol) [37]. Overall, CLNCs show controlled and prolonged drug release that assured long-term availability of the drugs in physiological fluids and preferentially in the tumor microenvironment due to EPR effect of the NPs for a particle size less than 200 nm. Furthermore, drug release of less than 50 % in 2 h is acceptable for efficient tumor growth inhibition *in vivo* [38].

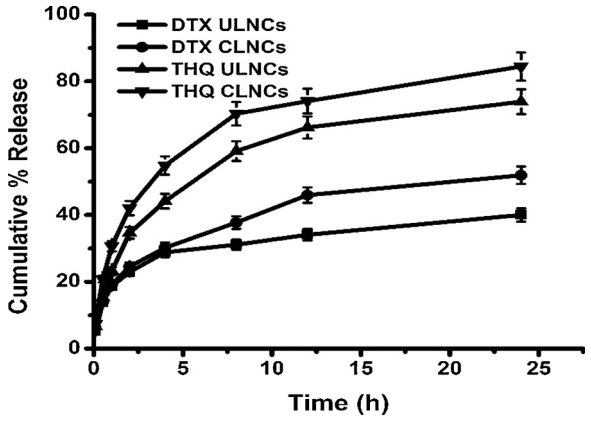

Fig. 5. *In-vitro* release profile of DTX and THQ from ULNCs and CLNCs. Values are presented as mean ± S.D (n = 3).

On fitting the release data into various kinetic models, Korsmeyer-Peppas model was followed with r^2 value of 0.942 and 0.988 for DTX, and 0.982 and 0.985 for THQ, from ULNCs and CLNCs, respectively. The calculated value of n (release exponent) was 0.14 (DTX ULNCs) and 0.16 (DTX CLNCs) for DTX, and 0.19 (THQ ULNCs) and 0.18 (THQ CLNCs) for THQ, suggesting a Fickian diffusional transport of both the drugs from the LNCs.

3.5. Hemolytic toxicity assay

The biocompatibility of nanocapsules with red blood cells (RBCs) was evaluated by quantifying the release of hemoglobin in the *in vitro* hemolysis test. The negative control (NS) produced negligible hemolysis due to its isotonic nature. However, the positive control (DW) showed 100 % hemolysis, as the RBCs lyse in a hypotonic medium. Hemolytic profiles of different concentrations of CLNCs revealed hemolysis ranging between 2.5 ± 0.2 % and 4.7 ± 0.2 % (table S4). A higher positive charge with the increasing concentration of LNCs resulted in a slightly higher hemolysis. Overall, the percentage hemolysis caused by LNCs was within the acceptable limit of < 5 % [14].

3.6. In vitro cell viability assay

The *in vitro* cell viability assay was conducted on two human breast carcinoma cell lines, MCF-7 and MDA-MB-231. The MCF-7 breast cancer cells express estrogen receptors (ERα), whereas MDA-MB-231, TNBC, cells are negative for estrogen receptor alpha (ERα), progesterone receptor, and human epidermal growth factor receptor 2 (HER2) [39]. As evident in Fig. 6.1, the cytotoxic effects of the treatment were dependent on the drug concentration, and incubation time. Free DTX solution exhibited 55.1 ± 3.3 % inhibition of the MCF-7 cells at 5 µM concentration, while THQ demonstrated a 42.4 ± 3.2 % cell inhibition at 40 µM concentration, with an IC50 value of 3.31 µM and 55.60 µM for DTX and THQ, respectively. However, it was observed that the DTX-LNCs produced a 69.1 ± 2.6 % and 74.5 ± 3.5 % cell inhibition at

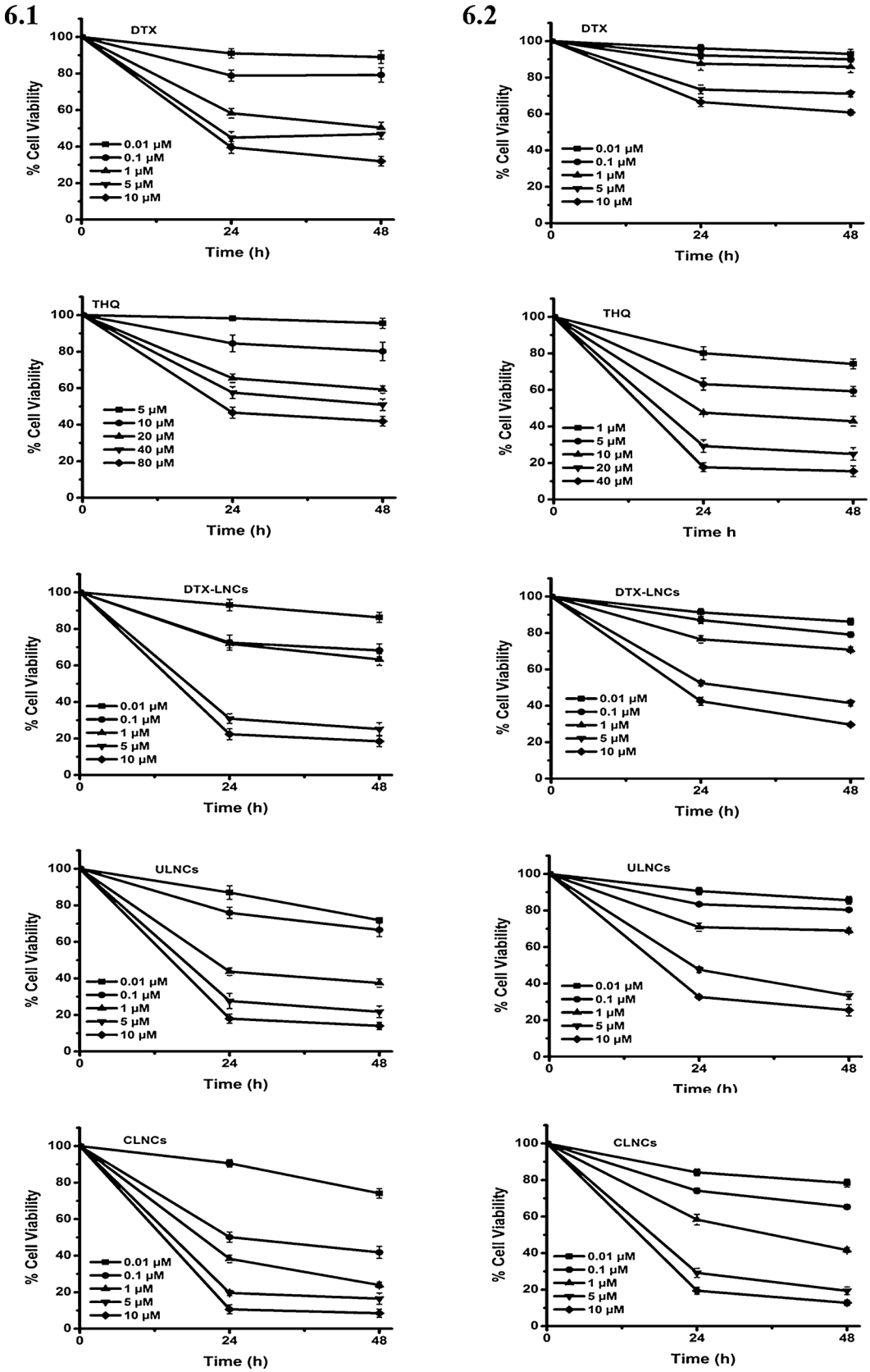

Fig. 6. Dose-dependent antiproliferative effect on MCF-7 breast cancer cells (6.1) and MDA-MB-231 triple negative breast cancer cells (6.2) by different treatments at 24 and 48 h incubation period. Cells were treated with DTX, THQ, DTX-LNCs, ULNCs, CLNCs at varied concentrations. The group treated with CLNCs produced greater cytotoxic effects compared to other treatments. The presence of THQ and development of LNCs sensitized the TNBC cells to DTX treatment. Values are reported as mean ± S.D. ($p < 0.05$).

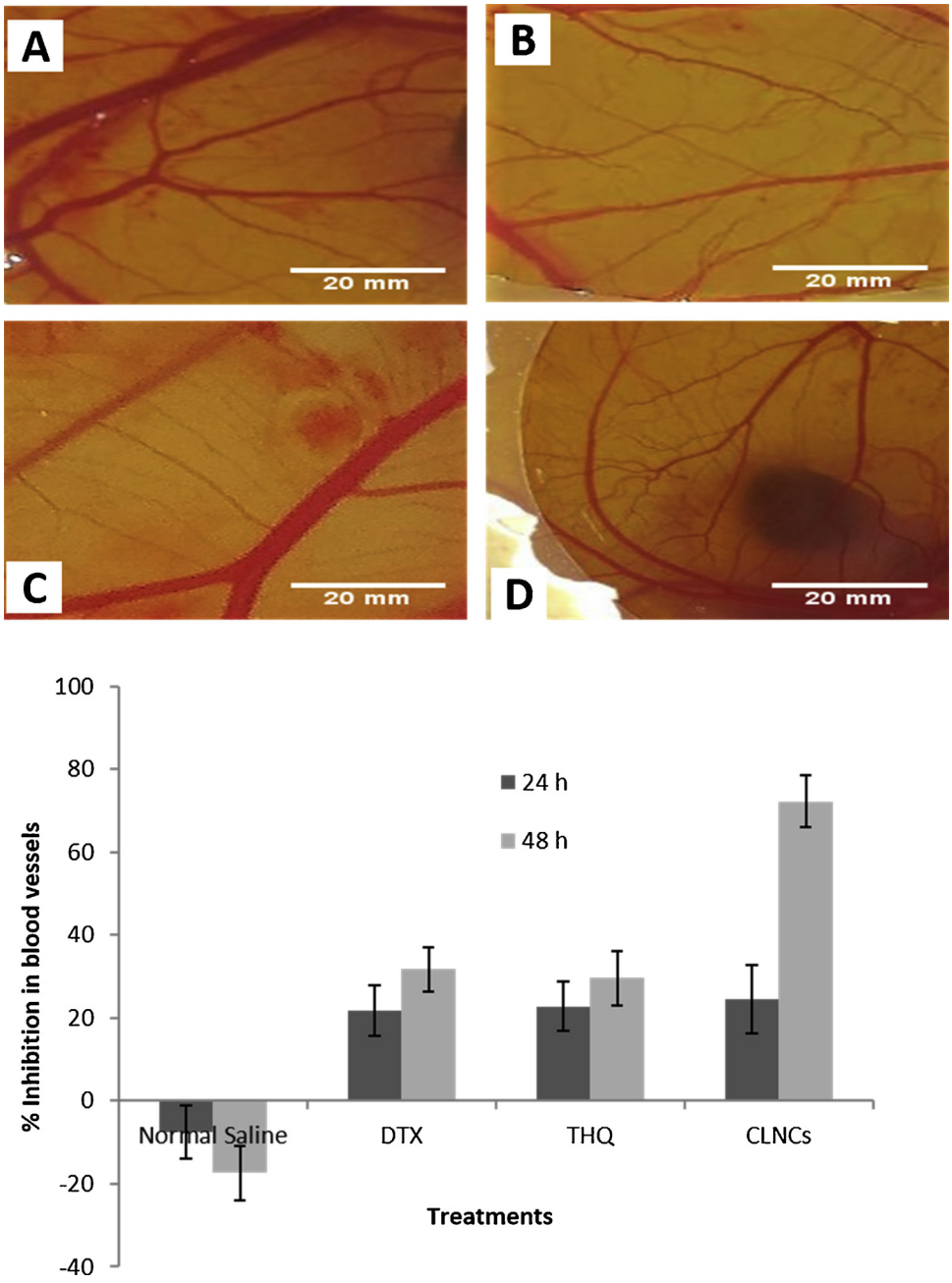

Fig. 7. Anti-angiogenic activity of DTX (A), THQ (B), CLNCs (C) and normal saline (D) on Chorioallantoic membrane (CAM) of 11-day-old chick embryo. The bar graph represents the time dependent effect of different treatments on blood vessels inhibition in the CAM assay. Data is represented as mean ± S.D. (n = 10).

24 h and 48 h, respectively with 5 μM DTX, which may be attributed to the sustained release of the entrapped drug from the LNCs. The effect was further enhanced in case of ULNCs, wherein 62.5 ± 2.3 % cells were inhibited with 1 μM drug concentration (IC50 of 0.45 μM after 48 h of study), which can be attributed to the anticancer activities of THQ, and the cytostatic effect of poloxamer on the cell lines [40]. A greater cell inhibition of 51.8 ± 3.5 % with a very low drug concentration of 0.1 μM was observed with the CLNCs compared to ULNCs, which was due to greater cellular uptake of CLNCs owing to the CS targeting the overexpressed CD44 receptors in the MCF-7 cells [14,41]. The cytotoxicity studies conducted on the TNBC cells, MDA-MB-231, revealed the lower activity of DTX (33.4 ± 2.5 % cell inhibition even at 10 μM DTX) compared to MCF-7 cells (Fig. 6.2). Notably, THQ which failed to produce potent effects in the MCF-7 cells, resulted in 57.2 ± 2.6 % cell inhibition in the MDA-MB-231 cells, even at the low concentration of 10 μM, with an IC50 value of 6.62 μM. THQ acts via peroxisome proliferators-activated receptor c-dependent pathway, reducing the levels of survivin, a multifunctional cell-protective protein overexpressed in most breast cancers, and hence induces apoptosis in breast cancer cells [42]. The percentage cell inhibition for the DTX-LNCs, ULNCs and CLNCs following 48 h of incubation period was reported to be 70.3 ± 1.1 %, 74.6 ± 3.1 % and 87.2 ± 1.5 %, respectively (Fig. 6.2). Thus, THQ and CLNCs sensitized the TNBC cells to DTX treatment. Previously, reports have demonstrated the increased exocytosis of the anti-tumor drugs through the endosomal vesicle recycling as one of the efflux mechanisms in the MDR tumor cells, which can be enhanced by the MDR related protein (P-gp). Thus, the shift in intracellular pH in the MDR tumor cells could possibly affect the rate of vesicular transport and exocytosis [17,43]. Here, the results indicated that the CS coating on the surface of nanocapsules, along with THQ and

P188 demonstrated superior cytotoxic performance in the TNBC and MCF7 cells.

3.7. In vivo anti-angiogenesis assay

Preclinical evaluation of the drug delivery systems (DDS) require the use of mammalian models which are expensive, time-consuming, and not easy to set up and evaluate. The administrative burden with respect to ethical and legal aspects further hinders their frequent usage. The increasing interest in the use of chick embryo as an *in vivo* model is related to its simplicity and low cost compared with mammalian models. Furthermore, the current laws regulating animal experimentation allows the usage of chick embryos without authorization from animal experimentation committees, on the grounds that experiments begin and end before hatching. Therefore, the CAM assay can be used routinely for evaluating the activity or toxicity of a drug and a DDS [22].

Abnormal angiogenesis plays a critical role in several pathologies including cancer. The results shown in Fig. 7 clearly indicate the anti-angiogenic effect of DTX, THQ, and CLNCs compared to that of the negative control (NS). The treatments induced localized disruptions in the CAM vessel, and produced an avascular zone in the vicinity of the treated region with pronounced results seen in case of CLNCs (Fig. 7). On the other hand, the CAM treated with NS displayed no response and showed a normal capillary network architecture (Fig. 7). The time-dependent response of CAM blood vessels to different treatments showed that the DTX- and THQ-treated groups showed an inhibition of 21.8 ± 6.1 % and 22.8 ± 6 %, respectively after 24 h of study. CLNCs produced an inhibition of 24.6 ± 8.2 % and 72.2 ± 6.3 % at 24 and 48 h, respectively, which was significant at 48 h. Endogenous expression of vascular endothelial growth factor (VEGF) at day 8–9 and 11–12, expression of fibroblast growth factor (FGF-2) at day 10–14, and hypoxia inducible factor-1 and -2 alpha (HIF-1α) at day 11 was observed in the CAM, and DTX and THQ are known to inhibit these pro-angiogenic factors, which corroborated the antiangiogenic effects observed with DTX- and THQ-loaded CLNCs [4,44,45].

4. Conclusion

We have developed and optimized the chitosan grafted CLNCs encapsulating DTX and THQ. The optimized CLNCs demonstrated a high payload of DTX and THQ, uniform particle size (< 200 nm), controlled release of the payloads, and remarkably higher cell cytotoxicity in MCF 7 cells and the resistant TNBC cells. The greater hemolysis with CLNCs, at acidic pH, represents the efficient endosome escape owing to the CS endosomal buffering capacity, that eventually increased the intracellular delivery of the dual payload. Further *in vivo* studies with the CLNCs demonstrated a superior antiangiogenic effect in the CAM assay. The performance of the developed nanocapsules is being further investigated in balb/c mice using Ehrlich ascites carcinoma model. Our results indicate that CLNCs are promising nanocarriers for the co-delivery of DTX and THQ, as a single pH responsive nanomedicine, for the effective targeted chemotherapy of normal and the resistant breast cancers.

Declaration of Competing Interest

The authors declare no conflict of interest.

Acknowledgements

Financial support was received from the Maulana Azad National Fellowship (No. F1-17.1/2014-15/MANF-2014-15-MUS-DEL-47855), provided by University Grants Commission, and the electron microscope facility of SAIF, AIIMS, New Delhi, India is duly acknowledged.

Appendix A. Supplementary data

Supplementary material related to this article can be found, in the online version, at doi:https://doi.org/10.1016/j.colsurfb.2019.110603.

References

[1] F. Nasrollahi, J. Varshosaz, A.A. Khodadadi, S. Lim, A. Jahanian-Najafabadi, Targeted delivery of docetaxel by use of transferrin/poly (allylamine hydrochloride)-functionalized graphene oxide nanocarrier, ACS Appl. Mater. Interfaces 8 (21) (2016) 13282–13293.
[2] S. Jain, G. Spandana, A.K. Agrawal, V. Kushwah, K. Thanki, Enhanced antitumor efficacy and reduced toxicity of docetaxel loaded estradiol functionalized stealth polymeric nanoparticles, Mol. Pharm. 12 (11) (2015) 3871–3884.
[3] C. Shi, Z. Zhang, F. Wang, X. Ji, Z. Zhao, Y. Luan, Docetaxel-loaded PEO–PPO–PCL/TPGS mixed micelles for overcoming multidrug resistance and enhancing antitumor efficacy, J. Mater. Chem. B 3 (20) (2015) 4259–4271.
[4] G.P. Mishra, B.S. Doddapaneni, D. Nguyen, A.W. Alani, Antiangiogenic effect of docetaxel and everolimus as individual and dual-drug-loaded micellar nanocarriers, Pharm. Res. 31 (3) (2014) 660–669.
[5] B. Cote, L.J. Carlson, D.A. Rao, A.W. Alani, Combinatorial resveratrol and quercetin polymeric micelles mitigate doxorubicin induced cardiotoxicity in vitro and in vivo, J. Control. Release 213 (2015) 128–133.
[6] A.L. Al-Malki, A.A.R. Sayed, Thymoquinone attenuates cisplatin-induced hepatotoxicity via nuclear factor kappa-β, BMC Complement. Altern. Med. 14 (1) (2014) 282.
[7] S. Zafar, L.M. Negi, A.K. Verma, V. Kumar, A. Tyagi, P. Singh, et al., Sterically stabilized polymeric nanoparticles with a combinatorial approach for multi drug resistant cancer: in vitro and in vivo investigations, Int. J. Pharm. 477 (1–2) (2014) 454–468.
[8] M. Anwar, S. Akhter, N. Mallick, S. Mohapatra, S. Zafar, M.M.A. Rizvi, et al., Enhanced anti-tumor efficacy of paclitaxel with PEGylated lipidic nanocapsules in presence of curcumin and poloxamer: in vitro and in vivo studies, Pharmacol. Res. 113 (2016) 146–165.
[9] S.Y. Eid, M.Z. El-Readi, M. Wink, Synergism of three-drug combinations of sanguinarine and other plant secondary metabolites with digitonin and doxorubicin in multi-drug resistant cancer cells, Phytomedicine. 19 (14) (2012) 1288–1297.
[10] H. Gali-Muhtasib, A. Roessner, R. Schneider-Stock, Thymoquinone: a promising anti-cancer drug from natural sources, Int. J. Biochem. Cell Biol. 38 (8) (2006) 1249–1253.
[11] M. Sagit, F. Korkmaz, A. Akcadag, M.A. Somdas, Protective effect of thymoquinone against cisplatin-induced ototoxicity, Eur. Arch. Otorhinolaryngol. 270 (8) (2013) 2231–2237.
[12] M.N. Nagi, M.A. Mansour, Protective effect of thymoquinone against doxorubicin–induced cardiotoxicity in rats: a possible mechanism of protection, Pharmacol. Res. 41 (3) (2000) 283–289.
[13] G.M. Suddek, N.A. Ashry, N.M. Gameil, Thymoquinone attenuates cyclophosphamide-induced pulmonary injury in rats, Inflammopharmacology 21 (6) (2013) 427–435.
[14] W. Rao, H. Wang, J. Han, S. Zhao, J. Dumbleton, P. Agarwal, et al., Chitosan-decorated doxorubicin-encapsulated nanoparticle targets and eliminates tumor reinitiating cancer stem-like cells, ACS Nano 9 (6) (2015) 5725–5740.
[15] S. Akhter, I. Ahmad, M.Z. Ahmad, F. Ramazani, A. Singh, Z. Rahman, et al., Nanomedicines as cancer therapeutics: current status, Curr. Cancer Drug Targets 13 (4) (2013) 362–378.
[16] M. Lavertu, S. Methot, N. Tran-Khanh, M.D. Buschmann, High efficiency gene transfer using chitosan/DNA nanoparticles with specific combinations of molecular weight and degree of deacetylation, Biomaterials 27 (27) (2006) 4815–4824.
[17] I. Richard, M. Thibault, G. De Crescenzo, M.D. Buschmann, M. Lavertu, Ionization behavior of chitosan and chitosan–DNA polyplexes indicate that chitosan has a similar capability to induce a proton-sponge effect as PEI, Biomacromolecules 14 (6) (2013) 1732–1740.
[18] J. Key, K. Park, Multicomponent, tumor-homing chitosan nanoparticles for cancer imaging and therapy, Int. J. Mol. Sci. 18 (3) (2017) 594.
[19] G.E. Box, D.W. Behnken, Some new three level designs for the study of quantitative variables, Technometrics 2 (4) (1960) 455–475.
[20] B.C. Evans, C.E. Nelson, S.Y. Shann, K.R. Beavers, A.J. Kim, H. Li, et al., Ex vivo red blood cell hemolysis assay for the evaluation of pH-responsive endosomolytic agents for cytosolic delivery of biomacromolecular drugs, JoVE J. Vis. Exp. (73) (2013) e50166.
[21] D. Mandracchia, G. Tripodo, A. Trapani, S. Ruggieri, T. Annese, T. Chlapanidas, et al., Inulin based micelles loaded with curcumin or celecoxib with effective anti-angiogenic activity, Eur. J. Pharm. Sci. 93 (2016) 141–146.
[22] A. Vargas, M. Zeisserlabouebe, N. Lange, R. Gurny, F. Delie, The chick embryo and its chorioallantoic membrane (CAM) for the in vivo evaluation of drug delivery systems⋆, Adv. Drug Deliv. Rev. 59 (11) (2007) 1162–1176.
[23] S.M. Jafari, E. Assadpoor, Y. He, B. Bhandari, Re-coalescence of emulsion droplets during high-energy emulsification, Food Hydrocoll. 22 (7) (2008) 1191–1202.
[24] N. Mallick, M. Anwar, M. Asfer, S.H. Mehdi, M.M.A. Rizvi, A.K. Panda, et al., Chondroitin sulfate-capped super-paramagnetic iron oxide nanoparticles as potential carriers of doxorubicin hydrochloride, Carbohydr. Polym. 151 (2016) 546–556.
[25] S.M.M. Modarres-Gheisari, R. Gavagsaz-Ghoachani, M. Malaki, P. Safarpour, M. Zandi, Ultrasonic nano-emulsification – a review, Ultrason. Sonochem. 52 (2019) 88–105.

[26] J. Carpenter, V.K. Saharan, Ultrasonic assisted formation and stability of mustard oil in water nanoemulsion: effect of process parameters and their optimization, Ultrason. Sonochem. 35 (2017) 422–430.
[27] L.M. Negi, M. Jaggi, S. Talegaonkar, A logical approach to optimize the nanostructured lipid carrier system of irinotecan: efficient hybrid design methodology, Nanotechnology 24 (1) (2013) 015104.
[28] A.S. Zidan, O.A. Sammour, M.A. Hammad, N.A. Megrab, M.J. Habib, M.A. Khan, Quality by design: understanding the formulation variables of a cyclosporine a self-nanoemulsified drug delivery systems by Box–Behnken design and desirability function, Int. J. Pharm. 332 (1–2) (2007) 55–63.
[29] A. Muheem, F. Shakeel, M.H. Warsi, G.K. Jain, F.J. Ahmad, A combinatorial statistical design approach to optimize the nanostructured cubosomal carrier system for oral delivery of ubidecarenone for management of doxorubicin-induced cardiotoxicity: in vitro–in vivo investigations, J. Pharm. Sci. 106 (10) (2017) 3050–3065.
[30] D. Liu, J. Li, H. Pan, F. He, Z. Liu, Q. Wu, et al., Potential advantages of a novel chitosan-N-acetylcysteine surface modified nanostructured lipid carrier on the performance of ophthalmic delivery of curcumin, Sci. Rep. 6 (1) (2016) 28796.
[31] R.H. Müller, M. Radtke, S.A. Wissing, Solid lipid nanoparticles (SLN) and nanostructured lipid carriers (NLC) in cosmetic and dermatological preparations, Adv. Drug Deliv. Rev. 54 (2002) S131–55.
[32] M. Huang, E. Khor, L.-Y. Lim, Uptake and cytotoxicity of chitosan molecules and nanoparticles: effects of molecular weight and degree of deacetylation, Pharm. Res. 21 (2) (2004) 344–353.
[33] H. Zhao, Q. Li, Z. Hong, Paclitaxel-loaded mixed micelles enhance ovarian cancer therapy through extracellular pH-triggered PEG detachment and endosomal escape, Mol. Pharm. 13 (7) (2016) 2411–2422.
[34] Q. Liu, J. Chen, J. Du, Asymmetrical polymer vesicles with a “Stealthy” outer corona and an endosomal-escape-accelerating inner corona for efficient intracellular anticancer drug delivery, Biomacromolecules. 15 (8) (2014) 3072–3082.
[35] A.K. Varkouhi, M. Scholte, G. Storm, H.J. Haisma, Endosomal escape pathways for delivery of biologicals, J. Control. Release 151 (3) (2011) 220–228.
[36] Y. Liu, D. Liu, L. Zhu, Q. Gan, X. Le, Temperature-dependent structure stability and in vitro release of chitosan-coated curcumin liposome, Food Res. Int. 74 (2015) 97–105.
[37] M.F. Sohail, M. Rehman, H.S. Sarwar, S. Naveed, O. Salman, N.I. Bukhari, et al., Advancements in the oral delivery of Docetaxel: challenges, current state-of-the-art and future trends, Int. J. Nanomed. 13 (2018) 3145.
[38] P. Zhang, H. Zhang, W. He, D. Zhao, A. Song, Y. Luan, Disulfide-linked amphiphilic polymer-docetaxel conjugates assembled redox-sensitive micelles for efficient antitumor drug delivery, Biomacromolecules 17 (5) (2016) 1621–1632.
[39] T. Ovcaricek, S. Frkovic, E. Matos, B. Mozina, S. Borstnar, Triple negative breast cancer - prognostic factors and survival, Radiol. Oncol. [Internet] (2011) [cited 2019 May 24];45(1). Available from: http://content.sciendo.com/view/journals/raon/45/1/article-p46.xml.
[40] E.V. Batrakova, A.V. Kabanov, Pluronic block copolymers: evolution of drug delivery concept from inert nanocarriers to biological response modifiers, J. Control. Release 130 (2) (2008) 98–106.
[41] K.K. Upadhyay, A.N. Bhatt, E. Castro, A.K. Mishra, K. Chuttani, B.S. Dwarakanath, et al., In vitro and in vivo evaluation of docetaxel loaded biodegradable polymersomes, Macromol. Biosci. (2010) n/a-n/a.
[42] K.M. Sutton, C.D. Doucette, D.W. Hoskin, NADPH quinone oxidoreductase 1 mediates breast cancer cell resistance to thymoquinone-induced apoptosis, Biochem. Biophys. Res. Commun. 426 (3) (2012) 421–426.
[43] J. van Adelsberg, Regulation of cell pH by Ca + 2-mediated exocytotic insertion of H + - ATPases, J. Cell Biol. 102 (5) (1986) 1638–1645.
[44] A. Vacca, D. Ribatti, M. Iurlaro, F. Merchionne, B. Nico, R. Ria, et al., Docetaxel versus paclitaxel for antiangiogenesis, J. Hematother. Stem Cell Res. 11 (1) (2002) 103–118.
[45] T. Yi, S.-G. Cho, Z. Yi, X. Pang, M. Rodriguez, Y. Wang, et al., Thymoquinone inhibits tumor angiogenesis and tumor growth through suppressing AKT and extracellular signal-regulated kinase signaling pathways, Mol. Cancer Ther. 7 (7) (2008) 1789–1796.